Continuous local material model for cut edge effects in soft magnetic materials

S. Elfgen, S. Steentjes, S. Böhmer, D. Franck and K. Hameyer
Institute of Electrical Machines
RWTH Aachen University, Germany
silas.elfgen@iem.rwth-aachen.de

***Abstract*—Shape giving production steps in the manufacturing of electrical machines often introduce plastic deformation and residual stress into the soft magnetic material, thusly decreasing the magnetic quality and locally increasing hysteresis losses in the vicinity of the cut edges. Different models have been published, aiming to describe the changing local magnetisation and loss behaviour. Current approaches often consider permeability deteriorations by subdividing the soft magnetic material into slices of different material properties. Three cut edge models are discussed here, whereof two describe the changed local polarisation and the third estimates the resulting global iron losses. This paper presents a continuous material model for an efficient numerical model of the local magnetisation. By replacing effortful sliced models, the continuous model is independent of the discretisation and converges in case of coarse meshes to the sliced model.**

***Index Terms*—continuous material model, cutting edge, soft magnetic material**

I. Introduction

Different manufacturing techniques such as laser cutting for prototyping or stamping during production affect the local magnetic characteristics in a negative way and further differ considerably in their effects on the local resulting iron losses [1]. Depending on geometrical, material and processing parameters along with the magnetic field strength, the iron losses resulting from different cutting techniques can differ by a factor of two or higher [1]–[3]. Determining the local magnetic properties of soft magnetic materials used for example in electrical machinery, therefore is an essential part to consider in design and finite element (FE) simulations. The different cutting techniques introduce mechanical stress into the material, resulting in a locally decreasing permeability [4], [5]. The influence of cut surface gets more pronounced with decreasing geometrical sizes leading to superposing areas of degraded permeability [3], [4]. To cope with continuous, locally changing material properties different models have been published describing local permeability distributions [6]–[8] or aiming at the resulting iron losses [9]. Current attempts approximate the different local material properties by subdividing the iron core of a model into slices [7], [8], [10]. The different material properties are homogeneous across the corresponding slices. The sliced approach lacks due to the constant material properties inside the subdivision in accuracy. Moreover a complicated modelling of slices arise during preprocessing.

In light of these drawbacks, this paper compares different cut surface models and presents a continuous material model, established in the numerical FE simulation to describe local distributed magnetic material properties. The model presented, is based on the model published in [11]. The paper is structured as follows. Section II briefly explains the material characterisations performed to identify model parameters and compare loss calculations with measurements. Section III compares and assesses three different models to consider cut surface effects in FE simulation. Section IV introduces the continuous material model, its implementation and results of FE simulations using this model. Hysteresis losses are calculated on the basis of the mentioned models and compared to loss measurements described in Section II. Exemplary hysteresis loss calculations are performed on a physically and technically relevant application, in order to underline the effect of locally varying magnetic material properties. Section V gives a brief discussion on the results along with an outlook for further studies.

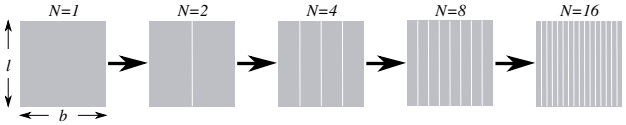

Fig. 1: Structure of single sheet sample preparation.

II. Material samples and characterisation

The required model parameters are identified using a set of single sheets of lamination. Starting with a basic sheet of $120\,\mathrm{mm}$ x $120\,\mathrm{mm}$ depicted in Figure 1, samples with smaller width are consecutively cut out of the basic square. Thereby, single samples equalling a width b of $120\,\mathrm{mm}$, $60\,\mathrm{mm}$, $30\,\mathrm{mm}$, $15\,\mathrm{mm}$, $10\,\mathrm{mm}$, $5\,\mathrm{mm}$ and $4\,\mathrm{mm}$ are produced. The material used for the sample set is M330-35A cutted by a CO2-Laser with a gas pressure of $10\,\mathrm{bar}$, using a speed of $8\,\frac{\mathrm{m}}{\mathrm{min}}$ and a power of $1700\,\mathrm{W}$. The specimens are magnetically characterised according to the IEC standard 60404-4 using a single sheet tester (SST), the field metric method and a quasi-static excitation. In order to compare the results of FE simulations to a measurable geometry, five toroidal cores are considered. The material and cutting parameters used equal those of the measured single sheets. The yoke diameter sizes are $15\,\mathrm{mm}$, $7.5\,\mathrm{mm}$, $5\,\mathrm{mm}$, $3.75\,\mathrm{mm}$ and $2.5\,\mathrm{mm}$. The iron core is stacked loosely and hold in shape using a Kapton tape

and the wiring.

III. Comparision of different models

In the following three models considering cut edge effects are compared and assessed. The first two models can be established in FE simulations describing the local permeability and the third one aiming at iron loss estimation.

A. Model 1

The first model, published in [12], is based on the conservation of energy. Derived therefrom the model approach is defined, with the measured polarisation J_{measured}, the strip width b and the modelled local polarisation distribution $\hat{J}_1(x)$. The local polarisation distribution is defined by the experimentally verified, continuously differentiable function, using the distance from the centre of the strip x, a material specific parameter A and the maximum of the local polarisation distribution $J_0(H)$ at constant magnetic field H.

$$J_{\mathrm{measured}} = \frac{1}{b}\int_{\frac{-b}{2}}^{\frac{b}{2}} J_0 \frac{cosh(A) - cosh(A\frac{x}{x_0})}{cosh(A) - 1}\, dx \qquad (1)$$

The relationship between a measured polarisation value and the modelled local distribution $\hat{J}_1(x)$ is achieved. This model provides a strip width dependent description of the local polarisation and requires a constant field strength across the specimen. Three model parameters are defined, namely parameters A, D the gradient at the cut edge $\frac{\mathrm{d}\hat{J}_1(x)}{\mathrm{d}x} = D$ and J_0. As the minimizing problem is not explicitly solvable a boundary condition is set. In [12] the limit of the modelled local polarisation is set to $J_0 \leq 1.1 \cdot J_{\mathrm{measured}}$. The basis of the constraint is not explained further, but the deviation between the locally modelled and the measured polarisation values rises with higher magnetic field strength. To improve the modelled material characteristic a new constraint is introduced limiting the maximum polarisation of smaller strip width $J_0(b)$ by the undamaged specimen $J_0(b = 120\,\mathrm{mm})$. The improved local polarisation curves are depicted in Figure 2(a). Having a description of the local polarisation the local permeability can be calculated considering a constant field strength.

B. Model 2

The second model, published in [11], describes the local material behaviour in terms of a locally dependent relative permeability. It involves three parameters, the permeability of an undamaged material sample $\mu_{\mathrm{r}}(H, N = 0)$, the maximum permeability drop at the cut surface $\Delta\mu_{\mathrm{cut}}(H)$ and the function $\eta(x)$ describing the local deterioration shape.

$$\mu_{\mathrm{r}}(H, x) = \mu_{\mathrm{r}}(H, N = 0) - \Delta\mu_{\mathrm{cut}}(H) \cdot \eta(x) \qquad (2)$$

The parameter N equals the amount of cuts applied to a specimen. The local deterioration profile $\eta(x)$ generally depends on the cutting method used. In case of mechanical cutting hyperbolic profiles are reported [4], [5], [12]. In case of laser cutting different profiles as well as non-symmetrical distributions are indicated in [13]. In the following, a parabolic permeability distribution is assumed described by $\eta(x)$.

$$\eta(x) = \left\{ \begin{array}{lll} 1 - \frac{x}{\delta} - a \cdot \frac{x}{\delta}(1 - \frac{x}{\delta}) & \forall & 0 \leq x \leq \delta \\ 0 & \forall & x > \delta \end{array} \right\} \qquad (3)$$

The model parameter δ indicates the depth of the area influenced by the cut surface, while the parameter a is a compression factor. The maximum permeability drop at the cut surface $\Delta\mu_{\mathrm{cut}}$ is defined in [11] as the difference between the permeability of the undamaged specimen and a damaged one. The expression should be constant for all measured strip widths, which is achieved by scaling through a function value $F(N)$. The parameter identification is based on the single sheet measurements mentioned in section II. The resulting characteristic permeability curves are depicted in Figure 2(b), comparing the modelled permeability to the measurements of different strip widths. In view of the parameter identification of the resulting material characteristics some adaptions have been made which are described in section IV.

C. Model 3

The third model, published in [9], correlates the total length of the cut l_{tot} of a specimen to the total mass m_{tot} and defines a cut surface factor S.

$$S = \frac{l_{\mathrm{tot}}}{m_{\mathrm{tot}}} = \frac{2 \cdot N_{\mathrm{s}} \cdot l}{m_{\mathrm{tot}}} \quad \text{with} \quad m_{\mathrm{tot}} = N_{\mathrm{s}} \cdot l \cdot b_{\mathrm{s}} \cdot d \cdot \rho \qquad (4)$$

The model aims on the resulting iron losses due to the influence of cut surfaces on the increasing proportion of hysteresis losses. A linear description of the resulting losses is achieved. Depicted in Figure 2(c) are the model results considering the SST specimens at quasi-static excitation. For different flux density values a linear description can be used in order to estimate the resulting iron losses.

D. Comparison of the moldels

The assessment of the three models is done in view of their applicability in FE simulation, as the aim is a continuous, local material description considering cut edge effects. All three models use SST measurements for model parameter identification. Model 1 and 2 assume a parabolic distribution of the polarisation, which is in accordance with other micromagnetic measurements [3], [13], [14]. Model 1 comprises three major drawbacks in view of applicability on physical applications as an electric machine. Firstly, the local material property depends on the strip with. Therefore, considering local material properties during FE calculations on an element basis requires to determine the total material width surrounding every element. This leads to problems in areas without parallel boundaries. Secondly, to identify the local material properties in terms of the permeability according to a defined strip width, it is necessary to previously know the expected polarisation, respectively the mean flux density across the area. This fact is the major drawback and clarifies the problems in terms of accuracy and applicability. Thirdly, a constant magnetic flux across the specimen is assumed which is inaccurate in case of a toroidal core. In contrast model 2 is a continuous

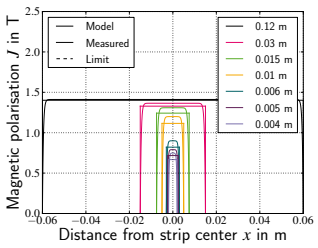

(a) Local polarisation $J(x)$ of model 1, limited by $J_0(b) \leq J_{\mathrm{measured}}(120\,\mathrm{mm})$.

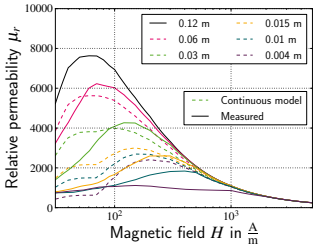

(b) Continuous material description of model 2.

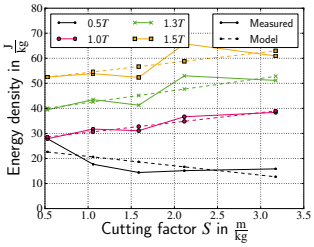

(c) Modelled and measured losses of toroidal cores, considering model 3.

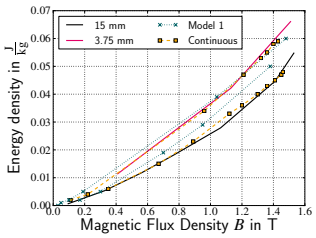

(d) Calculated and measured hysteresis losses of torodial cores considering Model 1 and the continuous model.

Fig. 2: Depicted are the result of the different cut edge models in (a), (b) and the resulting iron loss calculations considering model 3 in (c) and model 1 along with the proposed continuous model for exemplary toroidal cores in (d) .

material model describing material properties in dependency on the distance to the cut edge. As a consequence, it is possible to assign every element of a FE model a proper material characteristic depending on the magnetic field and the distance to the cut edge. Therefore, a consideration in FE simulation is possible and will be presented in the following. Model 3 provides a scaling factor or cut edge factor S using rising hysteresis losses along with a rising amount of cuts. Consequently the model can only be used in post processing to scale hysteresis losses. As depicted in Figure 2c the gradient is depending on the mean flux density and to estimate the resulting losses, at least two measuring points are required at a certain flux density for extrapolation. Summarizing, model 2 is currently the most suitable model to continuously describe local material properties in FE simulation and is considered in the following.

IV. Continuous Material Modelling in FE Simulation

To avoid the inaccuracies arising with sliced models in considering cut edge effects [7], [8], [10], a continuous cut edge Model based on model 2 is presented and used in FE simulation. As mentioned, parameter identification is performed on basis of single sheet measurements of different strip width. In the process of parameter identification accurate results are found when assuming parameter a to be constant $a = 1$. The local deterioration function $\eta(x)$ is limited by the quotient L/N, with L being the total width and N the number of cuts. The model does not cover a superposition of mechanical stress from both cutting surfaces in case of small strip width $\delta > \frac{b}{2}$, which results partly in an overestimation of the local permeability as seen in Figure 2(b) and leading to an unsymmetrical polarisation distribution. The interval boundaries are therefore replaced by $\frac{b}{2}$. In order to use the proposed continuous material model in FE simulations an algorithm assigning to each element a corresponding minimum distance to the cut surface is defined. The distance information is used as additional property of the mesh element. A material matrix is assembled with a defined number of non-linear material characteristics, which correspond to a particular distance to the cut surface. During simulation material characteristics of an FE are assigned by interpolating the matrix entries according to the proper FE distance to the cut edge.

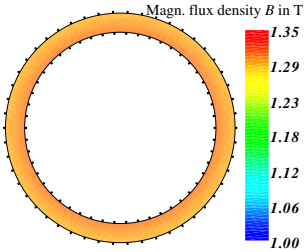

(a) Undamaged material characteristic.

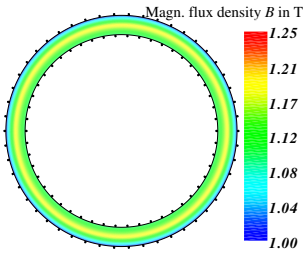

(b) Continuously modelled material characteristic.

Fig. 3: Resulting flux density distribution of a toroidal core of $15\,\mathrm{mm}$ yoke width, using a characteristic material curve without cutting effects 3(a) and (b) continuously modelled material behaviour.

A. Iron loss calculations

In the following section loss calculations on the toroidal cores are carried out, using model 1 and 2. As data basis for parameter identification the single sheet measurements are used. Hence, the toroidal cores are simulated considering the local material characteristics depicted in Figure 3. The lower mean flux density across the yoke along with the magnetic field dependency of the cut edge effect can be observed. The resulting hysteresis losses are calculated and compared to measurement results. With the identified hysteresis losses parameter a and α from the SST measurements, the hysteresis losses are calculated considering the local flux density $B(x)$. A dependency on the strip width b is considered in the loss parameters. The losses are calculated by integrating along the local flux density solutions $B(x)$ defined modelled on the soft magnetic area Ω.

$$E_{hyst} = \int_{\Omega} a_1(b) \cdot B(x)^{\alpha(b)} d\Omega \tag{5}$$

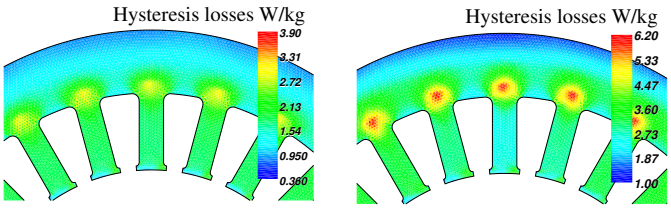

a) Unaffected b) Continuous model

Fig. 4: Comparison of the calculated hysteresis loss density on an unaffected stator (a) and in (b) a stator geometry the continuously modelled cut edge effects.

According to model 1 the the strip width and the expected mean flux density are needed to derive the local permeability. Unaffected simulations are carried out to verify the needed field strength for a certain flux density and strip width. The mentioned drawbacks in view of accuracy are obvious, as the expected mean flux density will be lower in an cut edge affected case. In the next step a parameter identification is carried out according to the assumed polarisation and strip width. As the model does not provide a magnetic field dependency and the local material characteristic is predefined by the model, only a single linear calculation step is performed. The resulting hysteresis losses of two toroidal cores considering model 1 and the presented continuous model are depicted in Figure 2(d). The calculated hysteresis losses of the proposed continuous model are in good agreement with the measured losses. Whereas model 1 overestimates the losses in case of the $15\,\mathrm{mm}$ toroidal core.

B. Application Example

In the following, effects of cut edge on the hysteresis losses of an exemplary physical application is presented, considering the local flux density distribution resulting from the introduced continuous model, together with the adapted hysteresis loss calculation from the previous subsection. Figure 4 demonstrates local hysteresis loss densities of an unaffected and a cut edge affected stator geometry. For the hysteresis loss calculation the model presented in [1] was used. In Figure 4 rising local loss densities can be observed in the vicinity of the stator tooth tips and the junction between stator teeth and yoke.

V. Conclusions

Three different approaches considering cut edge effects were compared in view of applicability in FE simulation and its results in view of hysteresis loss calculations. Measured single sheet specimens are used to identify the different model parameters. The advantages of the proposed continuous model which is only dependent on the distance to the cut edge are worked out. Hysteresis losses of toroidal cores are simulated employing the different models. In case of the continuous model measured and modelled overall hysteresis losses of the toroidal cores areas generally in good agreement. The applicability of the continuous model is applied to an exemplary stator geometry. In view of the continuous material description, two areas of further studies are necessary. With a rising amount of cuts, the permeability characteristic degenerates, leading to an overestimation of the local permeability. The maximum of the permeability curve shifts to higher field strength with a rising amount of cuts resulting in model inaccuracy, as the proposed model uses an exemplary permeability drop $\Delta\mu_{\mathrm{cut}}$ to describe different material characteristics.

References

[1] S. Steentjes, G. von Pfingsten, and K. Hameyer, "An Application-Oriented Approach for Consideration of Material Degradation Effects Due to Cutting on Iron Losses and Magnetizability," *IEEE Transactions on Magnetics*, vol. 50, no. 11, pp. 416–417, November 2014.

[2] A. Schoppa, J. Schneider, and C.-D. Wuppermann, "Influence of the manufacturing process on the magnetic properties of non-oriented electrical steels," *Journal of Magnetism and Magnetic Materials*, vol. 215-216, no. 0, pp. 74 – 78, 2000.

[3] P. Baudouin, M. D. Wulf, L. Kestens, and Y. Houbaert, "The effect of the guillotine clearance on the magnetic properties of electrical steels," *Journal of Magnetism and Magnetic Materials*, vol. 256, no. 13, pp. 32 – 40, 2003.

[4] F. Ossart, E. Hug, O. Hubert, C. Buvat, and R. Billardon, "Effect of punching on electrical steels: Experimental and numerical coupled analysis," *Magnetics, IEEE Transactions on*, vol. 36, no. 5, pp. 3137–3140, Sep 2000.

[5] G. Loisos and A. J. Moses, "Effect of mechanical and nd:yag laser cutting on magnetic flux distribution near the cut edge of non-oriented steels," *Journal of Materials Processing Technology*, vol. 161, no. 12, pp. 151 – 155, 2005, 3rd Japenese-Mediterranean Workshop on Applied Electromagnetic Engineering for Magnetic and Superconducting Materials and 3rd Workshop on Superconducting Flywheels.

[6] K. Fujisaki, R. Hirayama, T. Kawachi, S. Satou, C. Kaidou, M. Yabumoto, and T. Kubota, "Motor core iron loss analysis evaluating shrink fitting and stamping by finite-element method," *IEEE Transactions on Magnetics*, vol. 43, no. 5, pp. 1950–1954, 2007.

[7] M. Bali, H. De Gersem, and A. Muetze, "Finite-element modeling of magnetic material degradation due to punching," *Magnetics, IEEE Transactions on*, vol. 50, no. 2, pp. 745–748, Feb 2014.

[8] L. Vandenbossche, S. Jacobs, X. Jannot, M. McClelland, J. Saint-Michel, and E. Attrazic, "Iron loss modelling which includes the impact of punching, applied to high-efficiency induction machines," in *Electric Drives Production Conference (EDPC), 2013 3rd International*, Oct 2013, pp. 1–10.

[9] B. Hribernik, "Influence of cutting strains on the magnetic anisotropy of fully processed silicon steel," *Journal of Magnetism and Magnetic Materials*, vol. 26, no. 1-3, pp. 72 – 74, 1982.

[10] Z. Gmyrek and A. Cavagnino, "Analytical method for determining the damaged area width in magnetic materials due to punching process," in *IECON 2011 - 37th Annual Conference on IEEE Industrial Electronics Society*, Nov 2011, pp. 1764–1769.

[11] L. Vandenbossche, S. Jacobs, F. Henrotte, and K. Hameyer, "Impact of cut edges in magnetization curves and iron losses in e-machines for automotive traction," in *Proceedings of 25th World Battery, Hybrid and Fuel Cell Electric Vehicle Symposium & Exhibition, EVS*, Schenzhen, China, November 2010.

[12] Schoppa and A.P., "Einfluss der be- und verarbeitung auf die magnetischen eigenschaften von schlussgeglühtem, nichtkornorientiertem elektroband," Ph.D. dissertation, RWTH Aachen, 2001.

[13] R. Siebert, J. Schneider, and E. Beyer, "Laser cutting and mechanical cutting of electrical steels and its effect on the magnetic properties," *IEEE*, vol. 50, no. 4, pp. 1–4, 2008.

[14] E. G. Araujo, J. Schneider, K. Verbeken, G. Pasquarella, and Y. Houbaert, "Dimensional effects on magnetic properties of fe-si steels due to laser and mechanical cutting," *IEEE Transactions on Magnetics*, vol. 46, no. 2, pp. 213–216, Februar 2010.